Freestanding Nanostructures via Reactive Ion Beam Angled Etching

Haig A. Atikian,[1] Pawel Latawiec,[1] Michael J. Burek,[1] Young-Ik Sohn,[1]
Srujan Meesala,[1] Normand Gravel,[2] Ammar B. Kouki,[2] and Marko Lončar[1,*]

[1] *Harvard University, School of Engineering and Applied Sciences, 33 Oxford Street, Cambridge, USA*
[2] *École de Technologie Supérieure, LACIME Laboratory, Montréal, QC, Canada*

Freestanding nanostructures play an important role in optical and mechanical devices for classical and quantum applications. Here, we use reactive ion beam angled etching to fabricate optical resonators in bulk polycrystalline and single crystal diamond. Reported quality factors are approximately 30,000 and 286,000, respectively. The devices show uniformity across 25mm samples, a significant improvement over comparable techniques yielding freestanding nanostructures.

The fabrication of nanoscale electronic, optoelectronic and photonic devices requires high quality substrate materials. Heteroepitaxially grown substrates provide many device layer/substrate combinations, where a high quality crystalline device layer is grown on a disparate substrate. Among multilayer substrates, perhaps the most well known is silicon-on-insulator (SOI), which has proven to be an invaluable substrate for numerous nanoscale devices ranging from mechanical oscillators to integrated photonic devices. Heteroepitaxial substrates have the unique property of providing mechanical and optical isolation of the device layer from the substrate material. For nanomechanical structures such as suspended beams, cantilevers or membranes, mechanical degrees of freedom are typically achieved by selectively removing the material underneath the device layer with an appropriate wet or dry isotropic etch, suspending the structure above the substrate [1]. Similarly, nanophotonic devices require light confinement by total internal reflection off material boundaries in the heterostructure or again by suspending the structure in air. Consequently, due to material compatibility constraints in heteroepitaxial growth, there exists restrictions on device layer/substrate combinations for a wide range of materials such as $LiNbO_3$, SiC, GaN or diamond, to name a few [2–4]. Nevertheless, several innovative approaches to create comparable thin film on insulator technologies have emerged, such as crystal ion slicing [5–7], or thinning of bulk substrates [8–10]. Though these techniques have enabled the fabrication of nanophotonic and nanomechanical devices [11–14], reproducibility and uniform processing remain an issue for certain materials like diamond.

In contrast to thin film on insulator platforms, several other techniques have been developed where structures are etched directly from a bulk substrate by altering the angular trajectory of the ions impinging on the substrate surface. Techniques such as ion-sheath reactive ion etching (RIE) [15], focused ion beam (FIB) milling [16–19], Faraday cage angled-etching [20–24] or chemically assisted ion beam etching (CAIBE) [25], have been used to fabricate nanoscale photonic structures. A second category of techniques relies on isotropic etching via DC bias and process pressure variations to achieve an undercut structure [26–28]. Regardless of the technique, the commonality is a modification of the ion path striking the substrate.

In this letter, we explore a new technique creating freestanding photonic and mechanical nanostructures via reactive ion beam etching (RIBE), providing excellent uniformity and scaling processing. RIBE is a derivative of ion beam etching (IBE) or ion beam milling, where a broad area ion source is used to collimate and direct a uniform beam of high energy ions of a noble gas such as Ar, Xe or Ne towards a target to physically remove material via sputtering [29]. Ions are extracted from a plasma source by a set of electrically biased grids. Voltage applied to these grids controls the ion energy and the divergence of the ions within the beam. The collimated ion beam can then be directed towards an etch target at a prescribed angle [30–32]. Therefore, in an IBE system, the ion energy, flux and divergence can be independently set over a wide operational range enabling a uniquely unrestricted ion etching process. The use of reactive gases allows for more versatile etching of an expansive list of materials, otherwise difficult to etch with traditional IBE relying on physical sputtering. Essentially, an RIBE system is an IBE system whose inert gases have been replaced by reactive gases, such as chlorine or oxygen. CAIBE is a version of reactive ion beam etching, however it still uses an ion source of inert gases (Ar, Xe or Ne), while injecting a directed spray of the reactive gas towards the etch target. The kinetic energy of the inert gas ions exiting the ion source creates collisional fragmentation with the reactive gas and the resulting ions are directed towards the sample to perform the etch. Both techniques can yield great results, however the etch mask selectivity and overall wafer scale uniformity are better with RIBE [33].

Fig.1 depicts the fabrication procedure to create freestanding optical and mechanical nanostructures via reactive ion beam angled etching, from now referred to as (RIBAE). First, an etch mask is patterned onto the sample surface followed by a top down etch with the sample mounted on a rotating sample stage perpendicular to the ion beam path as seen in Fig.1(b,i). Once the desired ver-

* loncar@seas.harvard.edu

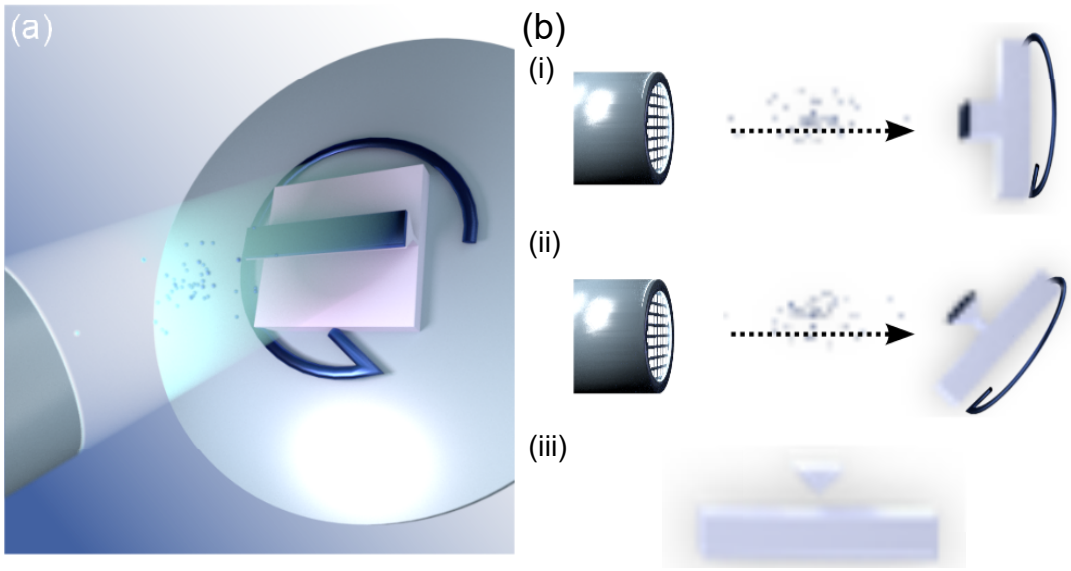

FIG. 1. (a) Graphical depiction of reactive ion beam angled etching (RIBAE). (b) RIBAE fabrication steps (i) Top-down etching of a sample mounted perpendicular to the ion beam path on a rotating sample stage. (ii) Sample tilted to obtain an acute angle between the sample and ion beam, uniformly etching underneath the etch mask. (iii) mask removal yielding freestanding nanostructures from a bulk substrate.

tical depth is achieved, the sample is tilted to obtain an acute angle with respect to the collimated ion beam, as seen in Fig.1(b,ii). Angled etching is performed with the sample stage rotating, uniformly etching underneath the mask. Once the desired undercut has been achieved the etch mask is removed yielding a triangular cross-section freestanding nanostructure as seen in Fig.1(b,iii).

To characterize the performance of the RIBAE technique, we fabricate diamond racetrack resonators in bulk polycrystalline diamond, similar to the ones found in [23]. An optical cavity is formed by a waveguide looped on itself and supports a resonance when the optical path length is an integer multiple of the wavelength. To achieve freestanding waveguides, vertical support structures are used to suspend the resonator above the substrate. This is accomplished by increasing the width of the waveguide at the support locations by 15%. The wider region requires more etch time to be completely etched from the substrate. This results in the racetrack resonator to be completely released from the substrate, while remaining attached at the vertical support locations by a thin diamond fin exhibiting minimal losses. More details on the optical mode analysis and propagation losses in the vertical supports can be found in [23].

We utilized 25mm diameter type IIa polycrystalline diamond wafer grown by CVD with $\sim$50μm grain boundaries obtained from Element 6. Polycrystalline diamond was used since large diameter wafers are readily available, as opposed to single crystal diamond. Diamond samples are first cleaned in a boiling mixture consisting of equal parts sulfuric, nitric and perchloric acid [34]. Hydrogen silsesquioxane (HSQ) resist is used to pattern racetrack resonator structures using 125keV electron-beam lithography and developed in a 25% tetramethylammonium hydroxide solution. The devices are etched by the RIBAE technique as outlined in Fig.1, with a Kaufman & Robinson 14cm diameter RF ICP ion beam source installed in an Intlvac system. RIBAE parameters are as follows: beam voltage 200V, accelerator voltage 26V, beam current 85mA, ICP power $\sim$155W, O_2 flow 37sccm and process pressure of 7.5x10^{-4} Torr. A non-immersed electron source neutralizer is used to neutralize the positive ions emitted from the ion source. The neutralizer is mounted on the side of the ion source with an emission current set to roughly x1.25 the ion source beam current and argon gas flow of 10sccm.

To determine the uniformity of the etching process across the entire diamond wafer, resonators are spaced apart by 19mm, indicated by the labels r1 and r2 as seen in Fig.2(a). Fiber taper coupling is used to characterize these structures [23], with Fig.2(b) indicating the fiber taper position during measurement. A typical normalized spectrum collected by a tunable laser and photodiode from the diamond racetrack resonators is shown in Fig.2(c), with a Lorentzian fit to resonance dips in r1 and r2 shown in Fig.2(d) exhibiting loaded quality factors of $\sim$30,000 and 24,000 respectively. Fig.2(e) plots the free spectral range (FSR) of both resonators r1 and r2 indicating excellent agreement with less than 5% deviation across the measured bandwidth. FSR is given by $\nu_{\mathrm{FSR}} = c/(n_g \times L)$, where c is the speed of light, n_g is the group index and L is the length of the cavity. Since the length of the resonators are identical for r1 and r2, the group index of both resonators must also be within the same tolerance, suggesting uniformity in the waveguide geometry. This validates the uniformity in the etch-

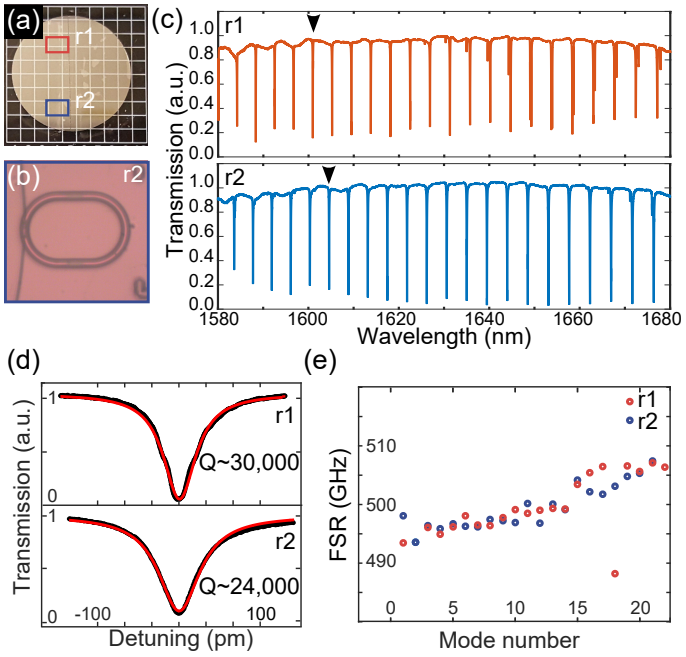

FIG. 2. (a) Optical micrograph of the 25mm polycrystalline diamond wafer, locations r1 and r2 mark the placement of diamond racetrack resonators separated by 19mm. (b) Optical micrograph indicating fiber taper coupling position. (c) Normalized broadband spectrum of diamond racetrack resonators r1 and r2 collected by fiber taper measurement. (d) Lorentzian fit (red) to the resonance positions marked by the arrows in panel (c), with a loaded quality factor of ∼30,000 and 24,000 for r1 and r2 respectively. (e) FSR comparison of diamond racetrack resonators r1 and r2 exhibiting less than 5% deviation. Outlier point on r1 indicates a position of a mode crossing for the resonator.

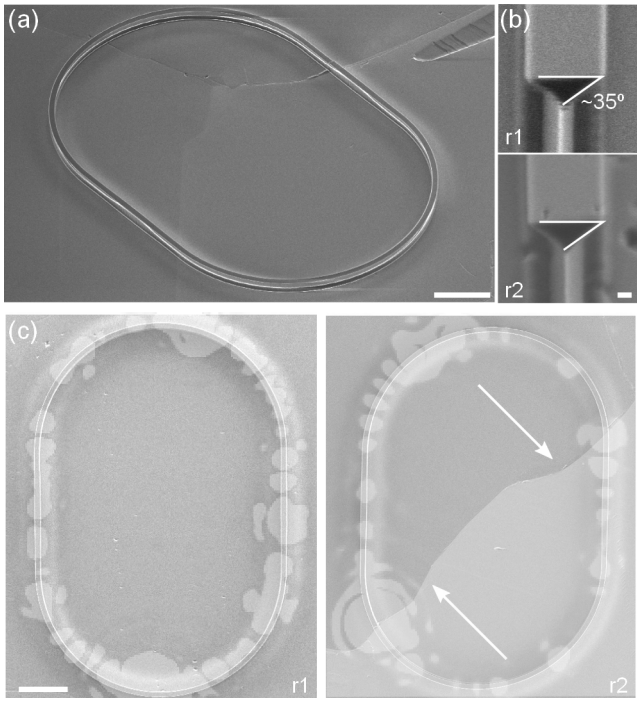

FIG. 3. (a) SEM image of diamond racetrack resonator etched in a bulk polycrystalline diamond, 10μm scale bar. (b) Cross sectional SEMs of exemplary freestanding devices in the locations adjacent to r1 and r2 exhibiting identical etch angles of 35°, 200nm scale bar. (c) Top down SEMs of resonators r1 and r2 with overlaid telecom scattered light when coupled on resonance, 10μm scale bar. Arrows point to the grain boundary line with a highlighted grain showing the intersection with the diamond racetrack resonator.

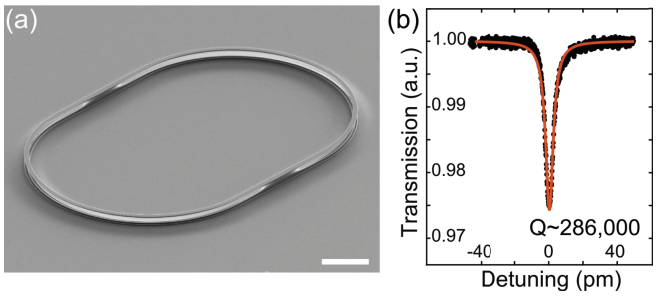

FIG. 4. (a) SEM image of a diamond racetrack resonator etched in a bulk single crystal diamond, 10μm scale bar. (b) Lorentzian fit (red) to a resonance dip with a loaded quality factor of ∼286,000.

ing profile across a wide area sample. This uniformity in etching is the key advantage of RIBAE compared to Faraday cage angled-etching, a similar technique which also produces freestanding devices of triangular cross section. As outlined in reference [22, 24], the Faraday cage exhibits variation in ion flux, angle and ion energy in relation to position in the cage, resulting in a pronounced etch gradient even across a sample of several millimeters. By contrast, in RIBAE the ion beam can be adjusted to have uniform ion flux and energy across the beam diameter allowing for uniform processing of large area samples.

Fig.3(a) shows an SEM of a diamond racetrack resonator fabricated in the 25mm polycrystalline diamond wafer. Clear grain boundaries can be seen in the diamond surface, which act as scattering points that consequently lower the quality factor one can obtain from polycrystalline samples [35]. Fig.3(b) shows cross section SEMs of exemplary freestanding devices in the locations adjacent to r1 and r2 exhibiting identical etch angles of 35°, further demonstrating the uniformity of the RIBAE technique across a large area sample. Fig.3(c) shows top down SEM images of resonators r1 and r2 with overlaid images of the scattered light captured with an infrared camera when the resonators are coupled on resonance. The location of a polycrystalline grain boundary is indicated by the arrows in the figure, coinciding with points of increased scattering when crossing the optical resonator.

To confirm that RIBAE is capable of producing high quality factor optical structures, we also fabricate identical resonators in 3mm x 3mm type IIa single crystal diamond substrates, Fig.4(a). Similar fiber taper mea-

surements are performed to characterize the optical properties of this device. Fig.4(b) presents the Lorentzian fit of a resonance dip with a quality factor of ∼286,000, comparable to the quality factors of previously realized triangular cross section devices using Faraday cage angled-etching. The quality factor is mainly determined by losses due to scattering, material absorption, losses to the substrate via support structures and waveguide bending losses. Since the geometry of the resonators are identical, higher quality factor resonators are achievable in single crystal diamond due to the lack of grain boundaries compared to polycrystalline diamond, which otherwise contribute to loss through geometric discontinuities (scattering) and material impurity (absorption). The quality factors and overall etch uniformity RIBAE affords opens up new possibilities for the scalable fabrication of diamond photonic devices.

In conclusion, we have presented a novel fabrication technique, RIBAE, to fabricate freestanding photonic nanostructures from bulk substrates across a 25mm diamater sample. RIBAE offers consistent etching conditions across large area samples allowing for uniform and reproducible processing of freestanding nanostructures. To characterize the performance of this new etching technique, 25mm polycrystalline bulk diamond samples are used to pattern racetrack resonators. Devices separated by 19mm exhibit identical optical properties from etch angle, FSR and optical quality factors, an improvement from similar structures fabricated by Faraday cage angled-etching where etch uniformity is difficult to achieve even across a mm length scale [22].

This work was performed in part at the Center for Nanoscale Systems (CNS), a member of the National Nanotechnology Coordinated Infrastructure Network (NNCI), which is supported by the National Science Foundation under NSF award no. 1541959. CNS is part of Harvard University. Fabrication was partially performed in the LACIME Laboratory at École de Technologie Supérieure. This work was supported in part by the Air Force Office of Scientific Research (MURI, grant FA9550-14-1-0389), the Defense Advanced Research Projects Agency (DARPA, W31P4Q-15-1-0013), STC Center for Integrated Quantum Materials, NSF Grant No. DMR-1231319, and NSF GOALI grant (1507508). P.L. was supported by the National Science Foundation Graduate Research Fellowship under Grant No. DGE1144152. The authors thank Daniel Twitchen and Matt Markham from Element Six for support with diamond samples.

[1] K. L. Ekinci and M. L. Roukes, Review of Scientific Instruments **76**, 061101 (2005).

[2] M. Herman, W. Richter, and H. Sitter, *Epitaxy: Physical Principles and Technical Implementation* (Springer, 2004).

[3] J. E. Ayers, *Heteroepitaxy of Semiconductors: Theory, Growth, and Characterization* (CRC Press, 2007).

[4] E. G. Bauer, B. W. Dodson, D. J. Ehrlich, L. C. Feldman, C. P. Flynn, M. W. Geis, J. P. Harbison, R. J. Matyi, P. S. Peercy, P. M. Petroff, et al., Journal of Materials Research **5**, 852 (1990).

[5] M. Levy, R. M. Osgood, R. Liu, L. E. Cross, G. S. Cargill, A. Kumar, and H. Bakhru, Applied Physics Letters **73**, 2293 (1998).

[6] M. K. Zalalutdinov, M. P. Ray, D. M. Photiadis, J. T. Robinson, J. W. Baldwin, J. E. Butler, T. I. Feygelson, B. B. Pate, and B. H. Houston, Nano Letters **11**, 4304 (2011).

[7] J. C. Lee, A. P. Magyar, D. O. Bracher, I. Aharonovich, and E. L. Hu, Diamond and Related Materials **33**, 45 (2013).

[8] B. J. M. Hausmann, B. Shields, Q. Quan, P. Maletinsky, M. McCutcheon, J. T. Choy, T. M. Babinec, A. Kubanek, A. Yacoby, M. D. Lukin, et al., Nano Letters **12**, 1578 (2012).

[9] C. Xiong, W. Pernice, K. K. Ryu, C. Schuck, K. Y. Fong, T. Palacios, and H. X. Tang, Opt. Express **19**, 10462 (2011).

[10] Y. Tao and C. Degen, Advanced Materials **25**, 3962 (2013), ISSN 1521-4095.

[11] P. Latawiec, V. Venkataraman, M. J. Burek, B. J. M. Hausmann, I. Bulu, and M. Lončar, Optica **2**, 924 (2015).

[12] C. Wang, M. J. Burek, Z. Lin, H. A. Atikian, V. Venkataraman, I.-C. Huang, P. Stark, and M. Lončar, Opt. Express **22**, 30924 (2014).

[13] P. Ovartchaiyapong, L. M. A. Pascal, B. A. Myers, P. Lauria, and A. C. B. Jayich, Applied Physics Letters **101**, 163505 (2012).

[14] P. Rath, S. Ummethala, C. Nebel, and W. H. P. Pernice, physica status solidi (a) **212**, 2385 (2015), ISSN 1862-6319.

[15] S. Takahashi, K. Suzuki, M. Okano, M. Imada, T. Nakamori, Y. Ota, K. Ishizaki, and S. Noda, Nature Mater. **8**, 721 (2009).

[16] T. M. Babinec, J. T. Choy, K. J. M. Smith, M. Khan, and M. Lončar, J. Vac. Sci. Technol. B **29**, 010601 (2011).

[17] I. Bayn, B. Meyler, J. Salzman, and R. Kalish, New Journal of Physics **13**, 025018 (2011).

[18] T. Zhong, J. M. Kindem, E. Miyazono, and A. Faraon, Nature Commun. **6**, 8206 (2015).

[19] T. Zhong, J. Rochman, J. M. Kindem, E. Miyazono, and A. Faraon, Opt. Express **24**, 536 (2016).

[20] B.-O. Cho, S.-W. Hwang, J.-H. Ryu, I.-W. Kim, and S.-H. Moon, Electrochem. Solid-State Lett. **2**, 129 (1999).

[21] M. J. Burek, N. P. de Leon, B. J. Shields, B. J. M. Hausmann, Y. Chu, Q. Quan, A. S. Zibrov, H. Park, M. D. Lukin, and M. Lončar, Nano Letters **12**, 6084 (2012).

[22] P. Latawiec, M. J. Burek, Y.-I. Sohn, and M. Lončar, J. Vac. Sci. Technol. B **34**, 041801 (2016).

[23] M. J. Burek, Y. Chu, M. S. Z. Liddy, P. Patel, J. Rochman, S. Meesala, W. Hong, Q. Quan, M. D. Lukin, and M. Lončar, Nature Commun. **5**, 5718 (2014).

[24] M. J. Burek, J. D. Cohen, S. M. Meenehan, N. El-Sawah, C. Chia, T. Ruelle, S. Meesala, J. Rochman, H. A. Atikian, M. Markham, et al., Optica **3**, 1404 (2016).

[25] C. C. Cheng, V. Arbet-Engels, A. Scherer, and E. Yablonovitch, Physica Scripta **1996**, 17 (1996).

[26] P. Vettiger, U. Staufer, D. Kern, and N. C. MacDonald, Microelectronic Engineering **32**, 49 (1996), ISSN 0167-9317.

[27] S. S. Walavalkar, A. P. Homyk, M. D. Henry, and A. Scherer, Nanoscale **5**, 927 (2013).
[28] B. Khanaliloo, M. Mitchell, A. C. Hryciw, and P. E. Barclay, Nano Letters **15**, 5131 (2015).
[29] H. R. Kaufman, *Applications of Broad-Beam Ion Sources: An Introduction* (Kaufmann Robinson,Inc., 2011).
[30] H. Gokan and S. Esho, Journal of Vacuum Science and Technology **18**, 23 (1981).
[31] M. A. Bsch, L. A. Coldren, and E. Good, Applied Physics Letters **38**, 264 (1981).
[32] W. Katzschner, A. Steckenborn, R. Lffler, and N. Grote, Applied Physics Letters **44**, 352 (1984).
[33] R. Shul and S. Pearton, *Handbook of Advanced Plasma Processing Techniques* (Springer, 2000).
[34] H. A. Atikian, A. Eftekharian, A. Jafari Salim, M. J. Burek, J. T. Choy, A. Hamed Majedi, and M. Lončar, Applied Physics Letters **104**, 122602 (2014).
[35] P. Rath, N. Gruhler, S. Khasminskaya, C. Nebel, C. Wild, and W. H. P. Pernice, Opt. Express **21**, 11031 (2013).

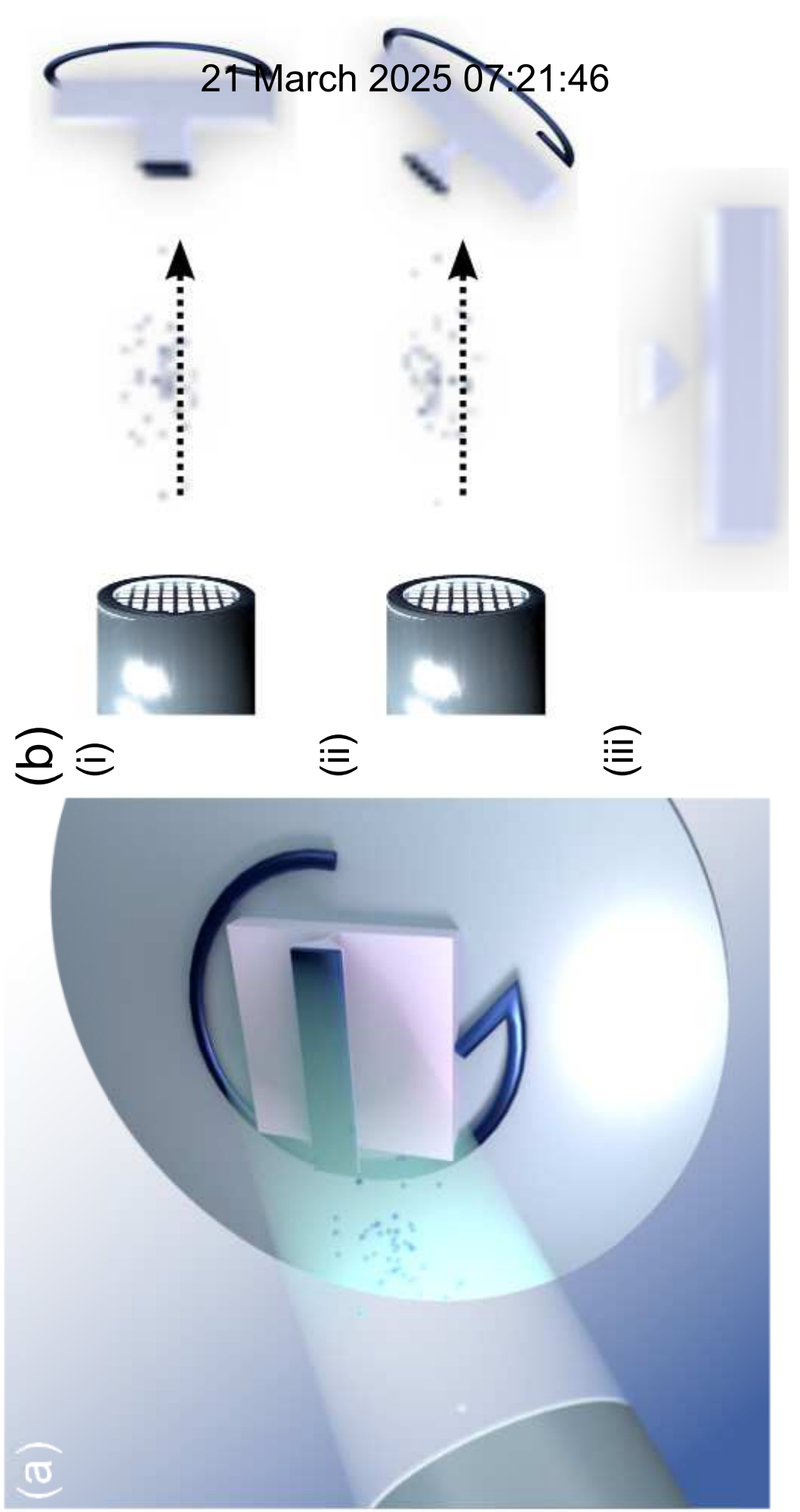

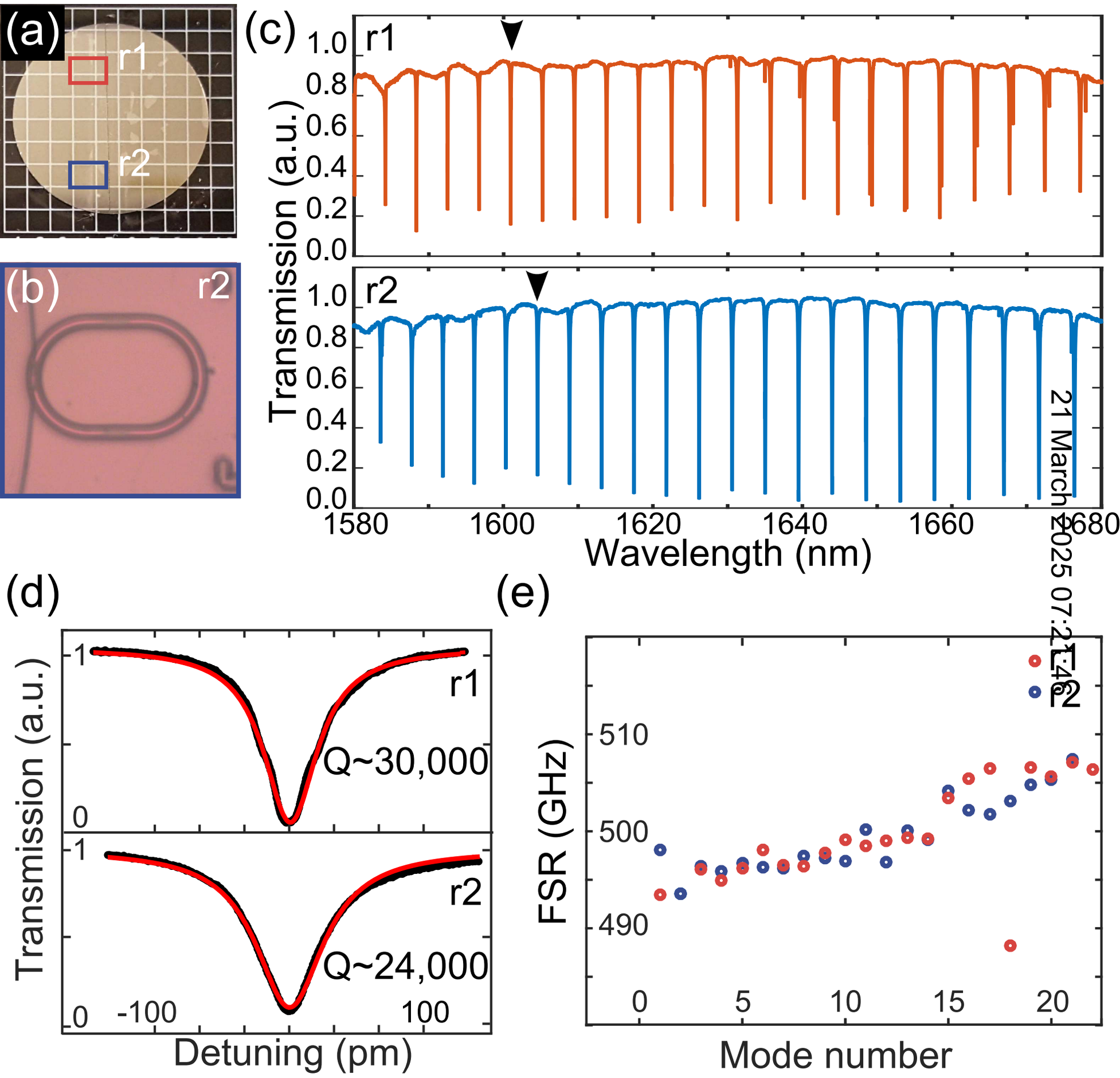
(a)
r1
r2
(b)
r2
(c)
r1
r2
Transmission (a.u.)
Wavelength (nm)
21 March 2025 07:21:46
(d)
r1
Q~30,000
r2
Q~24,000
Transmission (a.u.)
Detuning (pm)
(e)
FSR (GHz)
Mode number